Probabilistic Analysis of Commutation Failure in LCC-HVDC System Considering the CFPREV and the Initial Fault Voltage Angle

Yao, Wei; Liu, Chang; Fang, Jiakun; Ai, Xiaomeng; Wen, Jinyu; Cheng, Shijie

Published in:
IEEE Transactions on Power Delivery

DOI (link to publication from Publisher):
10.1109/TPWRD.2019.2925399

Publication date:
2020

Document Version
Accepted author manuscript, peer reviewed version

Probabilistic Analysis of Commutation Failure in LCC-HVDC System Considering the CFPREV and the Initial Fault Voltage Angle

Wei Yao, *Senior Member, IEEE*, Chang Liu, Jiakun Fang, *Senior Member, IEEE*, Xiaomeng Ai, *Member, IEEE*, Jinyu Wen, *Member, IEEE*, Shijie Cheng, *Life Fellow, IEEE*

***Abstract*—This paper investigates the in-depth mechanism of commutation failure for a line-commuted converter based high voltage direct current (LCC-HVDC) system. The commutation failure prevention control (CFPREV) and the initial fault voltage angle (IFVA) are considered from the view of the voltage-time area (VTA) in the analysis. It is revealed that the IFVA is among the dominant factors for commutation failures when the voltage drop of the inverter bus is relatively small, and CFPREV further intensifies the impact of the IFVA on commutation failures, while the fluctuation of the direct current plays a dominant role in commutation failures under a greater voltage reduction at the inverter bus. A quantitative division of the severity of AC faults is proposed to determine dominant factors for commutation failures. The relationship between the chance of commutation failures to occur and the IFVA is built, and the method used for computing probability of commutation failures is proposed. Influence of the dynamic of CFPREV output on our research is studied. Simulations based on a typical monopole LCC-HVDC system using PSCAD/EMTDC software are conducted to verify the correctness of the theoretic analysis and the effectiveness of the proposed computing methods.**

***Index Terms*—Line-commuted converter, high voltage direct current (HVDC), commutation failure, commutation failure prevention control (CFPREV), initial fault voltage angle (IFVA).**

NOMENCLATURE

β	supplementary angle of the firing angle in normal operation.
ΔU	commutating voltage.
$\Delta\varphi, \Delta\varphi_2$	phase shifts of the commutation voltage.
δ_{cf}	output of CFPREV.
$\gamma_{\min}$	the minimum extinction angle required for a commutation process.
θ	the IFVA.
A	the voltage-time area required for a commutation process .
$A(\theta)_{m-n(1)}$	The maximum voltage-time area that the AC system could provide in the first-round commutation process of $V_m \rightarrow V_n$.
$A_{m-n(2)}$	The maximum voltage-time area that the AC system could provide in the second-round commutation process of $V_m \rightarrow V_n$.
d	voltage drop of the fault phase.
I_{d}	direct current.
k	transformation ratio of the converter transformer.
L_{c}	commutating reactance.
t_1	firing instant of the analyzed valve.
$t_{2\max}$	the turning-off time of the analyzed valve when extinction angle equals to $\gamma_{\min}$.
$U''_{a0}, U''_{b0}, U''_{c0}$	the value of U''_a, U''_b, U''_c in normal operation.
$U'_{a0}, U'_{b0}, U'_{c0}$	the value of U'_a, U'_b, U'_c in normal operation.
$U''_{a1}, U''_{b1}, U''_{c1}$	the value of U''_a, U''_b, U''_c in phase-A fault.
$U'_{a1}, U'_{b1}, U'_{c1}$	the value of U'_a, U'_b, U'_c in phase-A fault.
U_A, U_B, U_C	three-phase voltages of the inverter bus.
U''_a, U''_b, U''_c	the phase voltages in the secondary side of the Y/$\triangle$ converter.
U'_a, U'_b, U'_c	the phase voltages in the secondary side of the Y/Y converter.
$V_1 \backsim V_{12}$	valves in a twelve-pulse converter.
$V_m \rightarrow V_n$	the commutation process from V_m to V_n.
V_m, V_n	valve m and valve n.

Manuscript received February 2, 2019; revised May 9, 2019; accepted June 24, 2019. This work was supported by the National Key Research and Development Program of China under Grant 2016YFB0900800 and the National Natural Science Foundation of China under Grant 51707077 and 51577075. Paper no. TPWRD-00152-2019 *(Corresponding author: Jiakun Fang.)*

W. Yao, J. K. Fang, X. M. Ai, J. Y. Wen, and S. J. Cheng are with State Key Laboratory of Advanced Electromagnetic Engineering and Technology, School of Electrical and Electronic Engineering, Huazhong University of Science and Technology, Wuhan, 430074, China. (email: w.yao@hust.edu.cn; jfa@hust.edu.cn; xiaomengai@hust.edu.cn; jinyu.wen@hust.edu.cn; sjcheng@hust.edu.cn)

C. Liu is with the Electric Power Research Institute of State Grid Sichuan Electric Power Company, Chengdu, 610072, China. (email: liuchang_sgo@qq.com)

I. INTRODUCTION

LCC-HVDC is widely used in power grid due to its advantages in bulk power transmission over long distance [1]–[3]. However, commutation failures of LCC-HVDC would pose great threats to the power grid [4]–[6]. Therefore, it is necessary to investigate the characteristic, mechanism and influential factors of commutation failures.

The mechanism and influential factors of commutation failures have been extensively investigated over the past decades. It is pointed out in [4] that commutation failures would happen unless the AC system is able to provide enough voltage-time area (VTA) required for the commutation process. Based on this theory, the influence of direct current, the commutation reactance, and the voltage drop of the inverter bus on commutation failures is studied in [4]. The influence of reactive power consumption on commutation failures is studied in [7],

This article has been accepted for publication in a future issue of this journal, but has not been fully edited. Content may change prior to final publication. Citation information: DOI 10.1109/TPWRD.2019.2925399, IEEE Transactions on Power Delivery

[8]. Among these influential factors, the reduction of voltage due to AC faults is the most frequently discussed, and it is even regarded as the only factor to identify commutation failures in a given system in [9]–[11].

However, simulations and commutation failure experience on actual systems show that one of the significant features of the commutation failure is its probabilistic characteristic. A quite large voltage reduction at the inverter bus might result in commutation failures, while a relatively small reduction might not [4], [12], [13]. This characteristic is remarkable especially after single-phase grounding faults in the inverter side [4]. The typical curve of commutation failure probability versus the voltage reduction is displayed in [4]. This probabilistic feature is simply attributed to the time when the AC fault is applied in [4], but the slope of this probabilistic curve is not quantitatively studied. In addition, commutation failure prevention control (CFPREV), a currently widely used method to mitigate commutation failures [14], [15], is able to alter the firing angle quite rapidly after AC faults and change the probability of commutation failures dramatically, but the effect of this control scheme is not considered in [4]. Ref. [16] analyzes the onset of commutation failures considering CFPREV, but the dynamic of CFPREV is not taken into consideration. In addition, the dominant factors for commutation failures are not studied. What the probabilistic characteristic of commutation failures would be like with consideration of the modern LCC-HVDC control scheme, and how to quantitatively depict this characteristic still need to be studied.

To answer this question, factors ranging from features of AC faults to LCC-HVDC control should be considered in the analysis of commutation failures. However, very little research has put all these factors together and analyzed to what extent these factors could influence commutation failures.

In this paper, the voltage angle between the fault instant and the reference instant is defined as the initial fault voltage angle (IFVA). The in-depth mechanism of commutation failures considering IFVAs, CFPREV, the fluctuation of the direct current, the voltage drop, the commutation reactance and other structural parameters is presented. Since single phase faults are the most common fault type, and the probabilistic characteristic is the most remarkable after single phase faults, in this paper we focus on the commutation failures after single-phase faults [4], [17]. This paper extends the work reported in [16], the main contributions of this paper are summarized as follows:

- The in-depth relationship between IFVAs and commutation failures is demonstrated considering CFPREV. This relationship shows that CFPREV intensifies the influence of the IFVA on commutation failures, thus making the probabilistic characteristic of commutation failures more remarkable.
- A quantitative division of the severity of AC faults is provided to determine dominant factors for commutation failures. This approach can be employed in the mitigation of commutation failures.
- The approach to calculate the range of IFVAs that could lead to commutation failures and the probability of commutation failures under a given voltage dip is proposed. This can be employed in the interpretation and prejudgement of the occurrence of commutation failures in simulations and practical operations.
- The dynamic of CFPREV reacting to a single-phase fault is studied. The influence of the time-delay of CFPREV output on our research is analyzed. This can be used for optimization of CFPREV parameters.

The remainder of this paper is organized as follows. In Section II, the VTA theory is introduced as a basis to analyze commutation failures. In Section III, commutation failures are studied considering CFPREV, the IFVA and other factors; the computing method of commutation failure probability is proposed. In Section IV, the proposed analyzing methods are verified by using the simulations performed on a HVDC model. Conclusions are drawn in Section V.

II. Commutation failure analysis for HVDC

A. Commutation failures and the VTA

In a commutation process, the commutating voltage of the converter valve which has just been turned off is supposed to keep positive for another short period of time. Otherwise, commutation failures happen [4].

Considering the fluctuation of I_d, if $V_m \rightarrow V_n$ has successfully completed a commutation process, we can obtain the following equation according to [12]:

$$L_c I_d(t_{2max}) + L_c I_d(t_1) \le \int_{t_1}^{t_{2max}} \Delta U \, dt \tag{1}$$

where, $I_d(t_1)$ and $I_d(t_{2max})$ represent the direct current at time t_1 and t_{2max}, respectively; L_c represents the commutation inductance. The left side of the above equation is referred to as A, namely the demand for VTA. The right side of the equation is referred to as the maximum VTA that the AC system could provide.

To study commutation failures in a practical LCC-HVDC system, it is of great importance to obtain ΔU before and after faults in the first place.

B. Commutating voltages before/after single-phase AC faults

The structure of a twelve-pulse converter which is widely used in practical LCC-HVDC systems is shown in Fig. 1 [18].

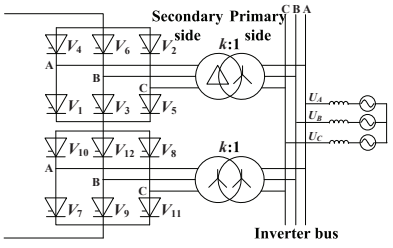

Fig. 1. The structure of a twelve-pulse converter.

As shown in Fig. 1, a twelve-pulse converter is made up of two Graetz Bridges connected in series. The wiring forms of converter transformers corresponding to each bridge are Y/△ and Y/Y, respectively; k is the transformer voltage ratio.

This article has been accepted for publication in a future issue of this journal, but has not been fully edited. Content may change prior to final publication. Citation information: DOI 10.1109/TPWRD.2019.2925399, IEEE Transactions on Power Delivery

Commutation processes of valves connected to transformers with different wiring forms show different characteristics. Considering the wring forms of converter transformers, the commutating voltages ΔU corresponding to different commutation processes are shown in Table I.

TABLE I
COMMUTATING VOLTAGES OF DIFFERENT COMMUTATION PROCESSES

Commutation Process	Wiring Forms of Transformers	Commutating Voltage ΔU
$V_6 \rightarrow V_2$	Y/△	U''_b
$V_3 \rightarrow V_5$		$-U''_b$
$V_4 \rightarrow V_6$		U''_a
$V_1 \rightarrow V_3$		$-U''_a$
$V_2 \rightarrow V_4$		U''_c
$V_5 \rightarrow V_1$		$-U''_c$
$V_7 \rightarrow V_9$	Y/Y	$U'_b - U'_a$
$V_9 \rightarrow V_{11}$		$U'_c - U'_b$
$V_{11} \rightarrow V_7$		$U'_a - U'_c$
$V_8 \rightarrow V_{10}$		$U'_c - U'_a$
$V_{10} \rightarrow V_{12}$		$U'_a - U'_b$
$V_{12} \rightarrow V_8$		$U'_b - U'_c$

When the AC system is operating normally, U''_a, U''_b, U''_c are $\sqrt{3}k$ times the value of U_A, U_B, U_C; U'_a, U'_b, U'_c are k times the value of U_A, U_B, U_C, respectively.

Assume that a single-phase (phase A) fault occurs in the AC system, and the phase-A voltage of the inverter bus declines d, while the voltages of phases B and C remain the pre-fault voltages.

After the fault, U'_a, U'_b, U'_c shown in Table I change from U'_{a0}, U'_{b0}, U'_{c0} to U'_{a1}, U'_{b1}, U'_{c1}, respectively:

$$\begin{cases} U'_{a1} = (1-d)U'_{a0} \\ U'_{b1} = U'_{b0} \\ U'_{c1} = U'_{c0} \end{cases} \tag{2}$$

The phasor diagram of pre-fault voltages and after-fault voltages are shown in Fig. 2(a). It can be concluded from Fig. 2(a) and Table I that $V_7 \rightarrow V_9$ and $V_{10} \rightarrow V_{12}$ are the most susceptible to commutation failures.

After the fault, U''_a, U''_b, U''_c in Table I change from U''_{a0}, U''_{b0}, U''_{c0} to U''_{a1}, U''_{b1}, U''_{c1}, respectively:

$$\begin{cases} U''_{a1} = (1-d)U''_{a0} + \Delta U_0 \\ U''_{b1} = U''_{b0} + \Delta U_0 \\ U''_{c1} = U''_{c0} + \Delta U_0 \end{cases} \tag{3}$$

where, ΔU_0 is a zero sequence voltage, which is caused by the wring form of the Y/△ transformer. This voltage alters the magnitude and orientation of U''_a, U''_b, and U''_c after the fault. It can be obtained from:

$$\Delta U_0 = \frac{1}{3} d U''_{a0} \tag{4}$$

The phasor diagram is shown in Fig. 2(b). Note that the commutating voltages U''_a, U''_b, and U''_c all decline; the zero-crossing point of U''_b moves forward, while the zero-crossing point of U''_c moves backward. Accordingly, it can be concluded from Fig. 2(b) and Table I that after a phase-A fault, $V_4 \rightarrow V_6$, $V_1 \rightarrow V_3$, $V_3 \rightarrow V_5$ and $V_6 \rightarrow V_2$ are the most susceptible to commutation failures.

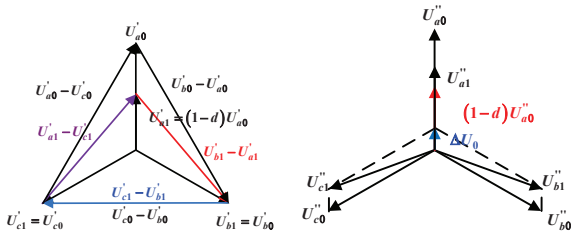

(a) Y/Y. (b) Y/Δ.

Fig. 2. Phasor diagram of voltages.

After obtaining the post-fault voltage deviation ΔU, we can substitute ΔU into (1), and determine whether commutation failures would happen or not.

In a practical LCC-HVDC system, various factors could influence the maximum VTA that the AC system could provide and the demand of the VTA, thus having an effect on the occurrence of commutation failures.

III. INFLUENCE MECHANISM OF IFVA AND CFPREV ON COMMUTATION FAILURES

A. Definition of IFVA

We divide the whole time horizon of interest into different time spans. Each time span takes 0.02s, starting when the phase-A voltage of the inverter bus crosses zero from a negative value to positive. The time span in which the fault occurs is denoted as SPAN1, and the firings in SPAN1 are referred to as the first-round firings. The time spans after SPAN1 are denoted as follow-up-round time spans, among which, the time span following SPAN1 is denoted as SPAN2, and the firings in SPAN2 are referred to as the second-round firings. In this paper, the IFVA is defined as the angle difference between the fault occurring instant and the starting point of SPAN1. We use θ to denote the IFVA. Since faults could occur at any instant indiscriminately, θ obeys uniform distribution.

As is analyzed above, ΔU is a piecewise function divided by the fault instant. Consequently, if the fault occurs during the period $[t_1, t_{2\max}]$, the maximum VTA that the AC system could provide is closely related to θ. As a result, the occurrence of commutation failures is influenced by θ.

B. Function of CFPREV

CFPREV is a widely used control scheme in LCC-HVDC. Its block diagram is shown in Fig. 3. It detects AC faults, and deducts δ_{cf} from the firing angle order in the inverter firing control according to the severity of the faults, thus advancing the firing instant and inhibiting commutation failures [12], [14]. In order to simplify the analysis and highlight the dominant characteristic of CFPREV, the time-delay of CFPREV output is firstly neglected in our analysis and then discussed in Section III-C5. When a single-phase fault occurs in the AC system, and the voltage drop of the fault-phase is d, δ_{cf} can be obtained by:

$$\delta_{\text{cf}} = \arccos(1 - k_1 d) \tag{5}$$

where, k_1 is a pre-defined parameter and is usually set as 0.075.

This article has been accepted for publication in a future issue of this journal, but has not been fully edited. Content may change prior to final publication. Citation information: DOI 10.1109/TPWRD.2019.2925399, IEEE Transactions on Power Delivery

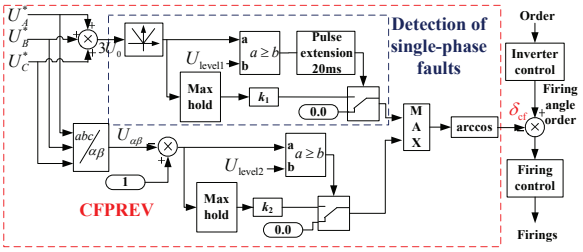

Fig. 3. Block diagram of CFPREV.

According to the VTA theory, CFPREV advances the firing instant t_1 in Eq. (1) to raise the maximum VTA that the AC system could provide. This helps to fulfill the necessary VTA to prevent the commutation failure. Since the CFPREV is triggered by AC faults, the moment when CFPREV is activated is influenced by the IFVA. This further intensifies the influence of the IFVA on commutation failures.

C. Analysis of Commutation Failures Considering CFPREV and IFVA

Owing to the periodicity of commutating voltages, Eq. (1) can be simplified as:

$$A \le \int_{t_1'}^{t_{2\max}'} \Delta U \, \mathrm{d}t \tag{6}$$

where $t_{2\max}' = t_{2\max} - t_0$, $t_1' = t_1 - t_0$; t_0 is the starting instant of SPAN1.

1) The maximum VTA of the first-round commutation process: Commutation processes in SPAN1 are referred to as the first-round commutation processes. After a phase-A fault in the AC system, the commutation processes of $V_3 \to V_5$, $V_{10} \to V_{12}$, $V_4 \to V_6$, $V_6 \to V_2$, $V_7 \to V_9$ and $V_1 \to V_3$ determine whether the commutation failures in the LCC-HVDC will occur or not. Due to the symmetrical characteristic of operation, the commutation processes of $V_3 \to V_5$, $V_{10} \to V_{12}$, $V_4 \to V_6$ are identical to those of $V_6 \to V_2$, $V_7 \to V_9$, $V_1 \to V_3$ respectively. Hence, only the commutation processes of $V_3 \to V_5$, $V_{10} \to V_{12}$ and $V_4 \to V_6$ are analyzed in this paper.

The maximum VTA that the AC system could provide in the first-round commutation process of $V_{10} \to V_{12}$ is denoted as $A(\theta)_{10-12(1)}$. Fig. 4 illustrates the $A(\theta)_{10-12(1)}$ under different θ interval. In Fig. 4, the shaded area represents $A(\theta)_{10-12(1)}$, and the phase shift of the commutation voltage $\Delta\varphi$ is [19]:

$$\Delta\varphi = \arctan\left(\frac{\sqrt{3}}{2(1-d)+1}\right) - \frac{\pi}{6} \tag{7}$$

In Fig. 4, t_1' and $t_{2\max}'$ in (6) are described by their corresponding radians.

The relationship between instants t_1', $t_{2\max}'$ and their corresponding radians θ_1, $\theta_{2\max}$ is:

$$\begin{cases} t_1' = \dfrac{\theta_1}{\omega} \\ t_{2\max}' = \dfrac{\theta_{2\max}}{\omega} \end{cases} \tag{8}$$

where ω is the electric angular velocity.

Note that θ_1 shown in Fig. 4 is influenced by the control scheme of LCC-HVDC and θ from the AC system. Due to the relatively slow reaction of the minimum extinction angle control in a typical LCC-HVDC control scheme, we assume that the reduction of the firing angle order in a HVDC control system is only caused by CFPREV. After the fault, CFPREV reduces the firing angle order by δ_{cf}. As illustrated in Fig. 5, the firings are generated by comparing the firing angle order with the value of the ramp generated by the phase locked oscillator. In Fig. 5, the abscissa represents the phase of U_A, and its original point is the start of SPAN1. The ramp represents the phase of line-to-line voltage U_{AB}. The pink dotted line is the firing angle order in normal operation, and the pink solid line represents the angle order after the fault. When θ belongs to different intervals, the advances of firings and θ_1 are different.

- $\theta \in [0, 5\pi/6 - \beta - \delta_{cf}]$

As illustrated in Fig. 4(a) and Fig. 5(a), when $\theta \in [0, 5\pi/6 - \beta - \delta_{cf}]$, the intersection point of the firing angle order and the phase ramp advances δ_{cf}. So the firing instant of V_{12} is $\theta_1 = 5\pi/6 - \beta - \delta_{cf}$. Due to the zero-crossing phase shift $\Delta\varphi$ caused by an unbalanced fault, $\theta_{2\max} = 5\pi/6 - \Delta\varphi - \gamma_{\min}$. Because ΔU, θ_1 and $\theta_{2\max}$ are not functions of θ, $A(\theta)_{10-12(1)}$ would not vary with the change of θ.

- $\theta \in [5\pi/6 - \beta - \delta_{cf}, 5\pi/6 - \beta]$

As illustrated in Fig. 4(b) and Fig. 5(b), when $\theta \in [5\pi/6 - \beta - \delta_{cf}, 5\pi/6 - \beta]$, the firing angle order crosses the phase ramp at θ, so the firing instant of V_{12} is just θ. It is easy to obtain $\theta_{2\max} = 5\pi/6 - \Delta\varphi - \gamma_{\min}$. With the increase of θ, θ_1 increases, whereas $\theta_{2\max}$ keeps the same, so $A(\theta)_{10-12(1)}$ decreases.

- $\theta \in [5\pi/6 - \beta, 5\pi/6 - \Delta\varphi - \gamma_{\min}]$

As illustrated in Fig. 4(c), when $\theta \in [5\pi/6 - \beta, 5\pi/6 - \Delta\varphi - \gamma_{\min}]$, the fault occurs in the commutation process. It can be seen from Fig. 5(c), the firing instant of V_{12} cannot be changed by CFPREV, so $\theta_1 = 5\pi/6 - \beta$, $\theta_{2\max} = 5\pi/6 - \Delta\varphi - \gamma_{\min}$. Because the fault occurs in the commutation process, ΔU is a piecewise function divided by the fault instant. Before the fault, $\Delta U = U_{a0}' - U_{b0}'$, while after the fault, $\Delta U = U_{a1}' - U_{b1}'$.Because $U_{a0}' - U_{b0}' > U_{a1}' - U_{b1}'$, $A(\theta)_{10-12(1)}$ increases with the increase of θ.

- $\theta \in [5\pi/6 - \Delta\varphi - \gamma_{\min}, 5\pi/6 - \Delta\varphi]$

As illustrated in Fig. 4(d) and Fig. 5(c), when $\theta \in [5\pi/6 - \Delta\varphi - \gamma_{\min}, 5\pi/6 - \Delta\varphi]$, the fault occurs after the commutation process. The occurrence of faults would not change ΔU and the firing instant of V_{12}. Through analyzing the commutating voltage, $\theta_{2\max} = 5\pi/6 - \Delta\varphi - \gamma_{\min}$. $A(\theta)_{10-12(1)}$ would not change with the vary of θ.

- $\theta \in [5\pi/6 - \Delta\varphi, 5\pi/6]$

As illustrated in Fig. 4(e) and Fig. 5(c), when $\theta \in [5\pi/6 - \Delta\varphi, 5\pi/6]$, the occurrence of faults would not change ΔU and the firing instance of V_{12}. However, the commutating voltage crosses zero at θ, which means $\theta_{2\max} = \theta - \gamma_{\min}$. With the increase of θ, θ_1 keeps the same, whereas $\theta_{2\max}$ increases, so $A(\theta)_{10-12(1)}$ increases with the increase of θ.

- $\theta \in [5\pi/6, 2\pi]$

This article has been accepted for publication in a future issue of this journal, but has not been fully edited. Content may change prior to final publication. Citation information: DOI 10.1109/TPWRD.2019.2925399, IEEE Transactions on Power Delivery

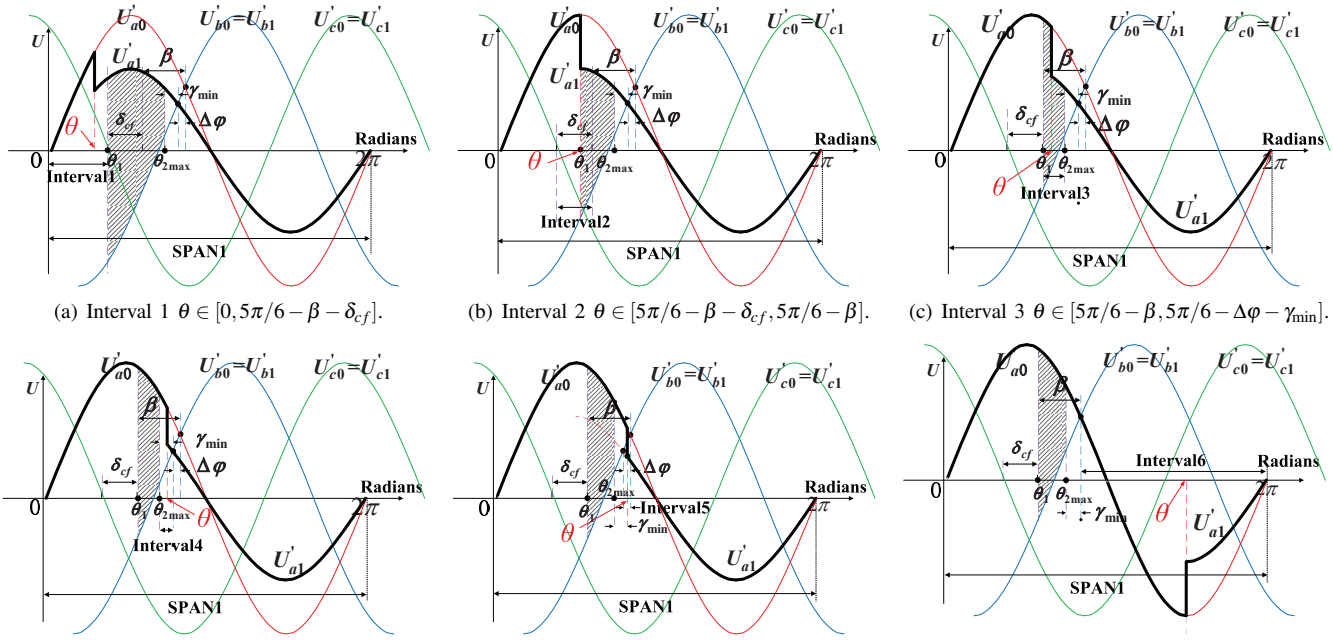

(a) Interval 1 $\theta \in [0, 5\pi/6-\beta-\delta_{cf}]$. (b) Interval 2 $\theta \in [5\pi/6-\beta-\delta_{cf}, 5\pi/6-\beta]$. (c) Interval 3 $\theta \in [5\pi/6-\beta, 5\pi/6-\Delta\varphi-\gamma_{\min}]$.

(d) Interval 4 $\theta \in [5\pi/6-\Delta\varphi-\gamma_{\min}, 5\pi/6-\Delta\varphi]$. (e) Interval 5 $\theta \in [5\pi/6-\Delta\varphi, 5\pi/6]$. (f) Interval 6 $\theta \in [5\pi/6, 2\pi]$.

Fig. 4. The maximum VTA corresponding to different IFVAs.

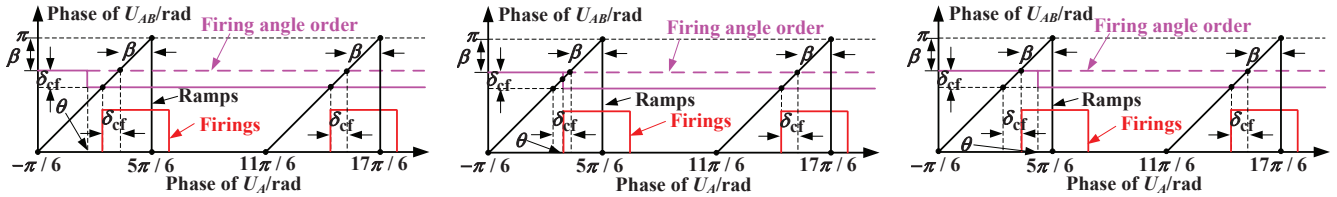

(a) $\theta \in [0, 5\pi/6-\beta-\delta_{cf}]$. (b) $\theta \in [5\pi/6-\beta-\delta_{cf}, 5\pi/6-\beta]$. (c) $\theta \in [5\pi/6-\beta, 2\pi]$.

Fig. 5. Principle of the firing control.

As illustrated in Fig. 4(f) and Fig. 5(c), when $\theta \in [5\pi/6, 2\pi]$, the fault occurs after the zero-crossing point of the commutating voltage. The firing instant of V_{12} is $5\pi/6-\beta$, $\theta_{2\max} = 5\pi/6-\gamma_{\min}$, $\Delta U = U'_{a0} - U'_{b0}$, and the fault would not influence the first-round commutation process of $V_{10} \rightarrow V_{12}$.

By applying Eq. (6), $A(\theta)_{10-12(1)}$ is given by:

$$A(\theta)_{10-12(1)} = \int_{t'_1}^{t'_{2\max}} \Delta U \mathrm{d}t \tag{9}$$

where t'_1, $t'_{2\max}$, ΔU are analyzed above and summarized in Table II of Appendix A. The t'_1, $t'_{2\max}$ and ΔU of $A(\theta)_{3-5(1)}$, $A(\theta)_{4-6(1)}$ are also summarized in in Tables III and IV of Appendix A, respectively.

2) Maximum VTA of the second-round commutation process: In addition to CFPREV, the minimum extinction angle control is also able to advance firings after AC faults [20], and the effect of this control scheme enhances with time. Moreover, when the voltage-dependent current-order limiter (VDCOL) scheme in HVDC is activated, I_{d} would be reduced, thus diminishing the demand for VTA [21]–[23]. These two control schemes are propitious to commutation processes. The effect of these control schemes increases with time, so among follow-up-round commutation processes, the second-round commutation process is the most vulnerable to commutation failures. Hence, we only analyze the second-round commutation process among follow-up-round commutation failures. In order to simplify our analysis, we neglect the effect of minimum extinction angle control and VDCOL in the second-round communication process.

The maximum VTA of the second-round $V_{10} \rightarrow V_{12}$ commutation process is shown in the shaded area of Fig. 6. It can be found that θ has no influence on commutation processes in the second round.

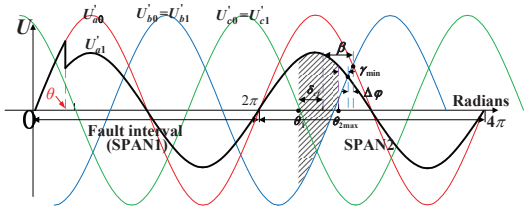

Fig. 6. The maximum VTA of the second-round $V_{10} \rightarrow V_{12}$ commutation process.

The θ_1, $\theta_{2\max}$ and ΔU of commutation processes $V_3 \rightarrow V_5$, $V_{10} \rightarrow V_{12}$ and $V_4 \rightarrow V_6$ in the second round are summarized in Appendix A. $A(\theta)_{3-5(2)}$, $A(\theta)_{10-12(2)}$ and $A(\theta)_{4-6(2)}$ are depicted in Table V of Appendix A.

3) Dominant factors influencing commutation failures: As can be seen from Eq. (6), the onset of commutation failures is influenced by various factors: the dynamic of I_{d}, the voltage drop at the inverter bus and the IFVA. We could discuss to what extent these factors influence commutation processes in

This article has been accepted for publication in a future issue of this journal, but has not been fully edited. Content may change prior to final publication. Citation information: DOI 10.1109/TPWRD.2019.2925399, IEEE Transactions on Power Delivery

different fault conditions.

- Scenario 1: AC faults are not severe

Take the commutation process of $V_{10}\rightarrow V_{12}$ as an example. The $A(\theta)_{10-12(1)}-\theta$ curve and $A(\theta)_{10-12(2)}-\theta$ curve under the scenario when the AC fault is not severe are illustrated in Fig. 7(a). It indicates that the faults that could cause commutation failures happen in the first-round commutation process. Due to the commutation reactance, I_{d} would not increase immediately. Hence, the direct current during the commutation process is simplified to remain as its rated value. The demand for the VTA can be described as:

$$A = 2L_{\mathrm{c}}I_{\mathrm{dn}} \tag{10}$$

where, L_{c} is the commutation reactance, I_{dn} is the rated value of I_{d}. Solving Eq. (6), the range of θ that could cause commutation failures is obtained. If the equation has solutions, the dominant factors that influence commutation failures are the IFVA and the voltage drop of the inverter bus; otherwise, the dominant factor is only the voltage drop of the inverter bus.

- Scenario 2: AC faults are severe

Fig. 7(b) is based on the scenario when the AC fault is severe, and $2L_{\mathrm{c}}I_{\mathrm{dn}}$ is so close to $\min(A_{m-n(2)})$(m-n=3-5, 10-12, 4-6) that a little fluctuation in I_{d} could influence the occurrence of commutation failures. Consequently, the fluctuation of I_{d} could not be neglected. The dominant factors for commutation failures are the IFVA, the voltage drop of the inverter bus and the fluctuation of I_{d}.

- Scenario 3: AC faults are very severe

Fig. 7(c) is based on the scenario when the AC fault is so severe that $2L_{\mathrm{c}}I_{\mathrm{dn}}$ is higher than $\min(A_{m-n(2)})$(m-n=3-5, 10-12, 4-6). In this scenario, no matter what time the fault occurs, commutation failures would definitely happen.

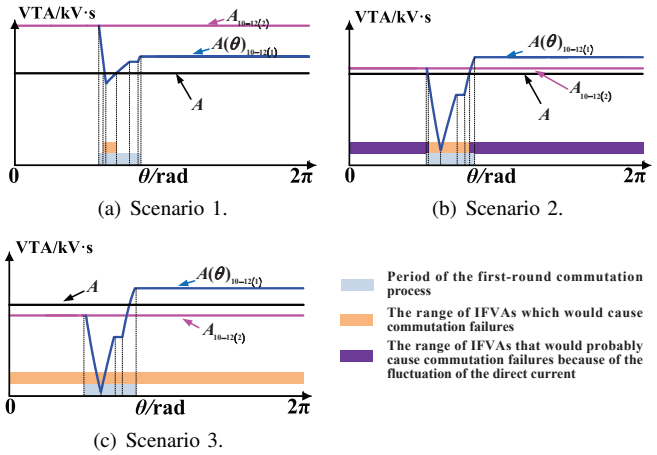

(a) Scenario 1. (b) Scenario 2.

(c) Scenario 3.

Fig. 7. Curves of $A(\theta)_{10-12(1)}-\theta$, $A(\theta)_{10-12(2)}-\theta$ and $A-\theta$.

Fig. 8 provides the procedure of the quantitative division of these three scenarios.

4) Computing method of the commutation failure probability: Considering CFPREV, the IFVA and I_{d}, the computing procedure of the commutation failure probability after a voltage-drop of d in phase A is shown in Fig. 9:

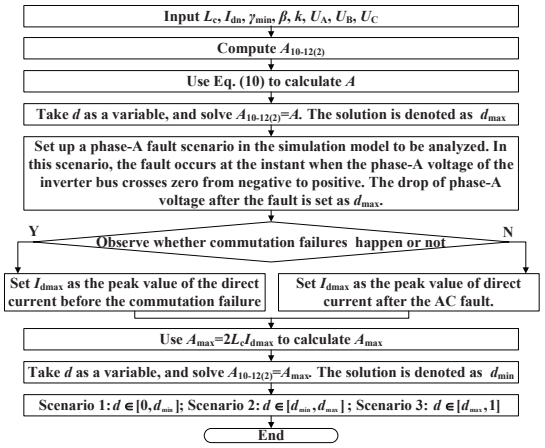

Fig. 8. Procedure of the quantitative division of three scenarios.

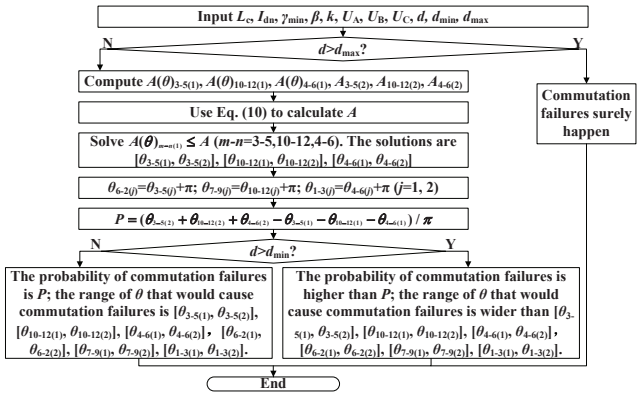

Fig. 9. Computing procedure of the commutation failure probability.

If the fault is a phase-B fault or a phase-C fault, the start of SPAN1 should be set as the zero-crossing instant of the fault-phase voltage. The computing procedures of the commutation-failure probability are identical to those of phase-A faults.

5) Influence of the dynamic of CFPREV output on commutation failures: As CFPREV works by detecting the AC faults, it takes time for its output to reach δ_{cf}. Since CFPREV output is assumed to be δ_{cf} the moment the fault occurs, it is necessary to find out whether our model for commutation failure analysis needs modifications.

According to the structure of CFPREV shown in Fig.3, ideal output of CFPREV under a single-phase fault occurred at θ is shown in Fig.10. In Fig.10, U_{level1} is the threshold to identify single-phase faults; $|3U_0|$ is the absolute value of the sum of three-phase instantaneous voltages; d is the voltage drop of the fault phase; δ_{cf} is the paramount of CFPREV output; θ is the initial fault voltage angel. It can be seen from Fig.10 that the dynamic of CFPREV output is closely related to threshold U_{level1} and θ.

Take commutation process $V_{10}\rightarrow V_{12}$ as an example to analyze the influence of the dynamic of CFPREV output on commutation failures.

If $d < U_{\mathrm{level1}}$, AC faults can't be detected by CFPREV. As a result, δ_{cf}=0. Under this circumstance, the commutation failure probability shows no difference with or without CFPREV.

If $d \geq U_{\mathrm{level1}}$, AC faults can be detected by CFPREV. The advancements of firings considering the dynamic of CFPREV

This article has been accepted for publication in a future issue of this journal, but has not been fully edited. Content may change prior to final publication. Citation information: DOI 10.1109/TPWRD.2019.2925399, IEEE Transactions on Power Delivery

are shown in Fig.10. θ' is the intersection point of $3U_0$ and threshold U_{level1}. $\theta' = \arcsin(U_{\text{level1}}/d)$. The influence of the dynamic of CFPREV output on commutation failures shows different characteristics when θ belongs to different ranges.

- $\theta \in [0, \theta']$

If $\theta \in [0, \theta']$, whenever the fault occurs, the output of CFPREV rises at θ' and reaches δ_{cf} at $\pi/2$. As illustrated in Fig.10(a), the firing is generated at $5\pi/6 - \beta - \delta_{cf}$. The time-delay of CFPREV output has no influence on the occurrence of commutation failures.

- $\theta \in [\theta', \pi/2]$

If $\theta \in [\theta', \pi/2]$, the output of CFPREV rises at θ and reaches δ_{cf} at $\pi/2$. As illustrated in Fig.10(b), the firing is also generated at $5\pi/6 - \beta - \delta_{cf}$. The time-delay of CFPREV output has no influence on the occurrence of commutation failures.

- $\theta \in [\pi/2, \theta'']$

If $\theta \in [\pi/2, \theta'']$, as illustrated in Fig.10(c), the output of CFPREV reaches its maximum at θ, but this maximum point is less than δ_{cf}. The intersection point lags behind the one when not considering the time-delay of CFPREV, which decreases $A(\theta)_{10-12(1)}$ in Table II.

- $\theta \in [\theta'', 2\pi]$

If $\theta \in [\theta'', 2\pi]$, as illustrated in Fig.10(d) and Fig.10(e), the time-delay of CFPREV output has no influence on commutation failures of $V_{10} \rightarrow V_{12}$.

As a result, the time-delay of CFPREV output decreases $A(\theta)_{10-12(1)}$ in Table II only when $\theta \in [\pi/2, \theta'']$. The closer θ is to $\pi/2$ and θ'', the smaller the decrease is. Since $V_{10} \rightarrow V_{12}$ is vulnerable to commutation failures when θ is around $5\pi/6 - \beta$, the influence of the time-delay of CFPREV output on commutation failures is little.

In conclusion, when $d < U_{\text{level1}}$, δ_{cf} should be modified into 0; when $d \geq U_{\text{level1}}$, the calculated commutation failure probability is smaller than the actual probability, but the distinction is little.

IV. Simulation Validation

A. Test System

A modified CIGRE HVDC benchmark system shown in Fig. 11 is used to verify the correctness of the analysis results. The HVDC system is rated at 500kV and 2000MW. The voltages of the inverter bus and the rectifier bus are both rated at 525kV. More detailed parameters of this test system are illustrated in Fig. 11, where S_{n} is the rated capacity of transformers, k is the transformation ratio, and x is the leakage reactance. In order to fulfill the potential of CFPREV, U_{level1} of CFPREV is set at a relatively low value.

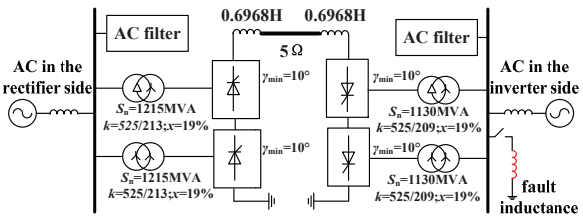

Fig. 11. The HVDC test system

B. Electromagnetic Transient Simulation Results

Electromagnetic transient simulations are performed by applying phase-A faults at the inverter bus. By adjusting the fault inductance, voltage dips with different percentage are applied to the inverter bus to represent different levels of severity with different remaining voltages in practice. These faults are applied with different IFVAs from 0 to 2π with a step size of 0.001 rad.

Fig. 12 provides the simulated results when $d = 30.2\%$, θ =0, 2 rad respectively.

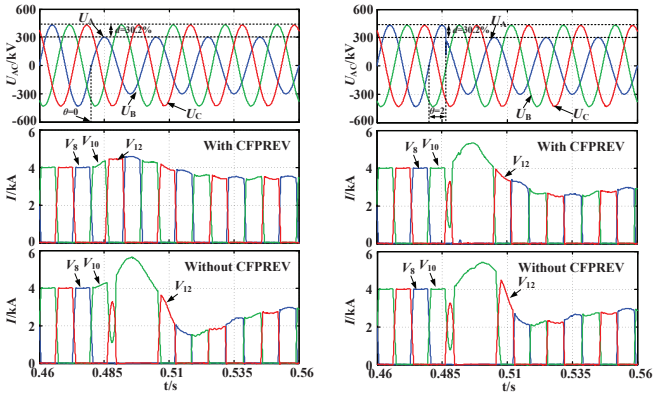

(a) $\theta = 0$ rad. (b) $\theta = 2$ rad.

Fig. 12. Simulation results ($d = 30.2\%$, $\theta = 0, 2$ rad).

It can be seen from Fig. 12 that if CFPREV is not applied, the commutation process of $V_{10} \rightarrow V_{12}$ fails when $\theta = 0$ and 2 rad. If CFPREV is applied, the commutation process of $V_{10} \rightarrow V_{12}$ fails only when $\theta = 2$ rad, while no commutation failure occurs when $\theta = 0$ rad. The commutation processes show differences with different θ. This is because the advancements of V_{12} firings are different even with the same CFPREV output.

Simulated probabilities of commutation failures are then obtained by calculating the proportion of cases that result in commutation failures in our simulation.

C. Relationship between CFPREV and the Influence of the IFVA on Commutation Failures

Fig. 13 provides the relationship between voltage drop and the probability of commutation failures with and without CFPREV. It can be seen from the results that, if CFPREV is not applied, commutation failures are likely to occur when the voltage-drop is larger than 10%, and it surely occurs if the voltage drop is over 15%; if CFPREV is applied, commutation failures are likely to occur when the voltage-drop is larger than 10%, and it surely occurs if the voltage drop is over 58%, which indicates that the probabilistic characteristic of commutation failures is more remarkable when CFPREV is applied. From our simulation, it can be obtained that this characteristic lies in IFVA, therefore it is proved that CFPREV enhances the influence of the IFVA on commutation failures.

D. Dominant Factors of Commutation Failures and the Quantitative Relationship between IFVA and Commutation Failures

1) Calculation results: Using the method proposed in Section III, we get A=0.187, $d_{\max} = 57.84\%$, $d_{\min} = 47.9\%$. The

This article has been accepted for publication in a future issue of this journal, but has not been fully edited. Content may change prior to final publication. Citation information: DOI 10.1109/TPWRD.2019.2925399, IEEE Transactions on Power Delivery

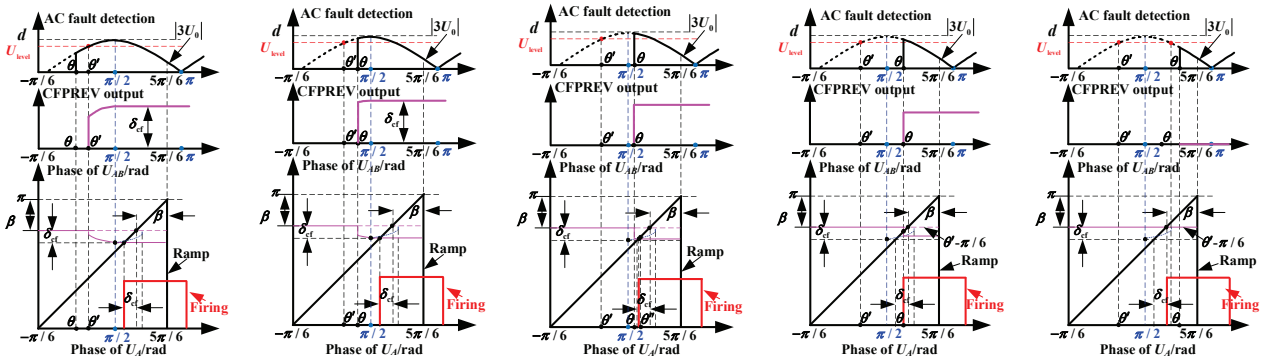

(a) $\theta \in [0, \theta']$. (b) $\theta \in [\theta', \pi/2]$. (c) $\theta \in [\pi/2, \theta'']$. (d) $\theta \in [\theta'', 5\pi/6-\beta]$. (e) $\theta \in [5\pi/6-\beta, 2\pi]$.

Fig. 10. The advancements of firings considering the dynamic of CFPREV.

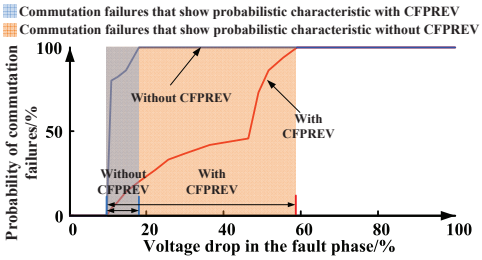

Fig. 13. Voltage drop-commutation failure probability curves.

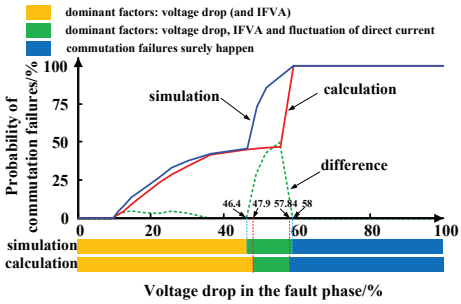

Fig. 14. Calculation and simulation results of probability of commutation failures.

range of IFVAs that could cause commutation failures and probabilities of commutation failures in the test system are also calculated. Based on our analysis, when d is between 0 and 47.9%, the dominant factors that could influence commutation failures are the voltage drop and the IFVA. When d is between 47.9% and 57.84%, the fluctuation of I_{d} also has great influence on commutation failures, so the actual probability of commutation failures would be higher than the calculated one. When d is greater than 57.84%, commutation failures would happen regardless of the IFVA.

2) Comparison of Calculation and Simulation results: As shown in Fig. 14, with CFPREV being applied, we compare the simulated and calculated probabilities of commutation failures under different remaining voltages of the inverter bus. Note that the modifications of δ_{cf} when $d < U_{\mathrm{level1}}$ is considered. It is obvious that if the voltage drop of the inverter bus is between 46.4% and 58%, the simulated probabilities are higher than the calculated ones. This range complies with the calculated $[d_{\min}, d_{\max}]$. According to our analysis, when d is between $d_{\min}$ and $d_{\max}$, not only the voltage drop and the IFVA, but also the fluctuation of I_{d} have dominant influence on commutation failures. Since in the calculation process, the value of I_{d} is simplified as a constant I_{dn}, the difference between simulated probabilities and the calculated ones just results from the fluctuation of I_{d}. When the voltage drop is not within this range, the simulated probabilities are consistent with calculated results. This is in accordance with our analysis that when d is not within $[d_{\min}, d_{\max}]$, the voltage drop and IFVAs can determine the occurrence of commutation failures.

With d being 10.91%, 14.69% and 30.2%, respectively, The simulated and calculated range of IFVAs that would cause commutation failures are shown in Fig. 15. The simulated results and the calculated ones are very close.

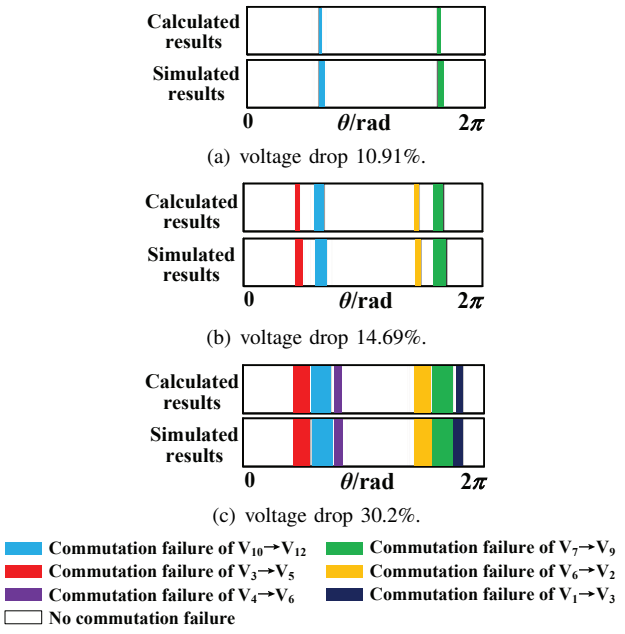

(a) voltage drop 10.91%.

(b) voltage drop 14.69%.

(c) voltage drop 30.2%.

Fig. 15. The range of IFVAs causing commutation failures in different voltage drops.

V. Conclusions

This paper analyzes the mechanism and probability of commutation failures in a LCC-HVDC system considering CFPREV and the IFVA. It is revealed that the dominant influential factors of commutation failures vary with the severity of AC faults. A quantitative division of the severity of AC faults is proposed to determine dominant factors for commutation failures and verified by simulations. It is pointed out that after a single-phase AC fault, if the voltage drop is relatively

This article has been accepted for publication in a future issue of this journal, but has not been fully edited. Content may change prior to final publication. Citation information: DOI 10.1109/TPWRD.2019.2925399, IEEE Transactions on Power Delivery

small, the IFVA is among the dominant influential factors of commutation failures. If the voltage drop is greater, the fluctuation of the direct current plays a more important role in commutation failures. This can provide guidance for the mitigation of commutation failures in future studies. It is also analyzed and verified by simulations that the reason for the probabilistic feature of commutation failures mainly lies in the IFVA, and this feature becomes more remarkable when CFPREV is applied. The proposed method in this paper can calculate the probability of commutation failures and the range of IFVAs that could cause commutation failures considering the effect of CFPREV. The influence of the dynamic of CFPREV output on our analysis is also researched. Since existing literature has not taken CFPREV into consideration in the analysis of commutation failures, this paper can better interpret commutation failures. Simulations are conducted based on a typical HVDC test system to validate the effectiveness of the proposed method. The simulation results of the test system comply with our analysis results.

APPENDIX A

$$\Delta\varphi_2 = \arccos\left(\frac{(U''_{b1})^2 + (U''_{b0})^2 - (\Delta U_0)^2}{2\left|U''_{b1}\right|\left|U''_{b0}\right|}\right) \tag{11}$$

TABLE II
INTEGRATION VARIABLES FOR $A(\theta)_{10-12(1)}$

IN VL	θ	ΔU	Limits of Integration	
			t'_1	$t'_{2\max}$
1	$[0, \frac{5\pi}{6}-\beta-\delta_{cf}]$	U'_{a1}-U'_{b1}	$\frac{\frac{5\pi}{6}-\beta-\delta_{cf}}{\omega}$	$\frac{\frac{5\pi}{6}-\Delta\varphi-\gamma_{\min}}{\omega}$
2	$[\frac{5\pi}{6}-\beta-\delta_{cf}, \frac{5\pi}{6}-\beta]$	U'_{a1}-U'_{b1}	$\frac{\theta}{\omega}$	$\frac{\frac{5\pi}{6}-\Delta\varphi-\gamma_{\min}}{\omega}$
3	$[\frac{5\pi}{6}-\beta, \frac{5\pi}{6}-\Delta\varphi-\gamma_{\min}]$	U'_{a0}-U'_{b0}	$\frac{\frac{5\pi}{6}-\beta}{\omega}$	$\frac{\theta}{\omega}$
		U'_{a1}-U'_{b1}	$\frac{\theta}{\omega}$	$\frac{\frac{5\pi}{6}-\Delta\varphi-\gamma_{\min}}{\omega}$
4	$[\frac{5\pi}{6}-\Delta\varphi-\gamma_{\min}, \frac{5\pi}{6}-\Delta\varphi]$	U'_{a0}-U'_{b0}	$\frac{\frac{5\pi}{6}-\beta}{\omega}$	$\frac{\frac{5\pi}{6}-\Delta\varphi-\gamma_{\min}}{\omega}$
5	$[\frac{5\pi}{6}-\Delta\varphi, \frac{5\pi}{6}]$	U'_{a0}-U'_{b0}	$\frac{\frac{5\pi}{6}-\beta}{\omega}$	$\frac{\theta-\gamma_{\min}}{\omega}$
6	$[\frac{5\pi}{6}, 2\pi]$	U'_{a0}-U'_{b0}	$\frac{\frac{5\pi}{6}-\beta}{\omega}$	$\frac{\frac{5\pi}{6}-\gamma_{\min}}{\omega}$

TABLE III
INTEGRATION VARIABLES FOR $A(\theta)_{3-5(1)}$

IN VL	θ	ΔU	Limits of Integration	
			t'_1	$t'_{2\max}$
1	$[0, \frac{4\pi}{6}-\beta-\delta_{cf}]$	-U''_{b1}	$\frac{\frac{4\pi}{6}-\beta-\delta_{cf}}{\omega}$	$\frac{\frac{4\pi}{6}-\Delta\varphi_2-\gamma_{\min}}{\omega}$
2	$[\frac{4\pi}{6}-\beta-\delta_{cf}, \frac{4\pi}{6}-\beta]$	-U''_{b1}	$\frac{\theta}{\omega}$	$\frac{\frac{4\pi}{6}-\Delta\varphi_2-\gamma_{\min}}{\omega}$
3	$[\frac{4\pi}{6}-\beta, \frac{4\pi}{6}-\Delta\varphi_2-\gamma_{\min}]$	-U''_{b0}	$\frac{\frac{4\pi}{6}-\beta}{\omega}$	$\frac{\theta}{\omega}$
		-U''_{b1}	$\frac{\theta}{\omega}$	$\frac{\frac{4\pi}{6}-\Delta\varphi_2-\gamma_{\min}}{\omega}$
4	$[\frac{4\pi}{6}-\Delta\varphi_2-\gamma_{\min}, \frac{4\pi}{6}-\Delta\varphi_2]$	-U''_{b0}	$\frac{\frac{4\pi}{6}-\beta}{\omega}$	$\frac{\frac{4\pi}{6}-\Delta\varphi_2-\gamma_{\min}}{\omega}$
5	$[\frac{4\pi}{6}-\Delta\varphi_2, \frac{4\pi}{6}]$	-U''_{b0}	$\frac{\frac{4\pi}{6}-\beta}{\omega}$	$\frac{\theta-\gamma_{\min}}{\omega}$
6	$[\frac{4\pi}{6}, 2\pi]$	-U''_{b0}	$\frac{\frac{4\pi}{6}-\beta}{\omega}$	$\frac{\frac{4\pi}{6}-\gamma_{\min}}{\omega}$

TABLE IV
INTEGRATION VARIABLES FOR $A(\theta)_{4-6(1)}$

IN VL	θ	ΔU	Limits of Integration	
			t'_1	$t'_{2\max}$
1	$[0, \pi-\beta-\delta_{cf}]$	U''_{a1}	$\frac{\pi-\beta-\delta_{cf}}{\omega}$	$\frac{\pi-\gamma_{\min}}{\omega}$
2	$[\pi-\beta-\delta_{cf}, \pi-\beta]$	U''_{a1}	θ/ω	$\frac{\pi-\gamma_{\min}}{\omega}$
3	$[\pi-\beta, \pi-\gamma_{\min}]$	U''_{a0}	$\frac{\pi-\beta}{\omega}$	θ/ω
		U''_{a1}	θ/ω	$\frac{\pi-\gamma_{\min}}{\omega}$
4	$[\pi-\gamma_{\min}, 2\pi]$	U''_{a0}	$\frac{\pi-\beta}{\omega}$	$\frac{\pi-\gamma_{\min}}{\omega}$

TABLE V
INTEGRATION VARIABLES FOR $A_{3-5(2)}$,$A_{10-12(2)}$,$A_{4-6(2)}$

Voltage-time Area	ΔU	Limits of Integration	
		t'_1	$t'_{2\max}$
$A_{3-5(2)}$	-U''_{b1}	$\frac{4\pi/6-\beta-\delta_{cf}}{\omega}$	$\frac{4\pi/6-\Delta\varphi_2-\gamma_{\min}}{\omega}$
$A_{10-12(2)}$	U'_{a1}-U'_{b1}	$\frac{5\pi/6-\beta-\delta_{cf}}{\omega}$	$\frac{5\pi/6-\Delta\varphi-\gamma_{\min}}{\omega}$
$A_{4-6(2)}$	U''_{a1}	$\frac{\pi-\beta-\delta_{cf}}{\omega}$	$\frac{\pi-\gamma_{\min}}{\omega}$

REFERENCES

[1] F. Wang, T. Q. Liu, and X. Y. Li, "Decreasing the frequency of HVDC commutation failures caused by harmonics," *IET Power Electron.*, vol. 10, no.2, pp. 215-221, Oct. 2017.

[2] Y. Xue, X. P. Zhang, and C. H. Yang, "Commutation failure elimination of LCC HVDC systems using thyristor-based controllable capacitors," *IEEE Trans. Power Delivery.*, vol. 33, no. 3, pp. 1448-1458, Jun. 2018.

[3] J. Wu, H. Li, G. Wang, and Y. Liang, "An improved traveling-wave protection scheme for LCC-HVDC transmission lines," *IEEE Trans. Power Delivery.*, vol. 32, no.1, pp. 106-116, Jan. 2017.

[4] C. V. Thio, J. B. Davies, and K. L. Kent, "Commutation failures in HVDC transmission systems," *IEEE Trans. Power Delivery*, vol. 11, no.2, pp. 946-957, Apr. 1996.

[5] R. Devarapalli and R. K. Pandey, "Analysis of weak AC system interface with multi-infeed HVDC," in *Proc. Int. Conf. Computing, Electronics and Electrical Tech.*, Mar. 2012, pp. 138-144.

[6] X. Wang, Y. Bai, Q. Chen, Y. Gao, J. Luo, and Y. Zhang, "A new interpretation of commutation failure risk in multi-infeed HVDC systems," in *Proc. IEEE Conf. Energy Internet and Energy System Integration.*, Nov. 2017, pp. 1-5.

[7] S. Mirsaeidi and X. Z. Dong, "An enhanced strategy to inhibit commutation failure in line-commutated converters," *IEEE Trans. Industrial Electronics.*, 2019, in press.

[8] Y. Xue and X. P. Zhang, "Reactive power and AC voltage control of LCC HVDC system with controllable capacitors," *IEEE Trans. Power Syst.*, vol. 32, no.1, pp. 753-764, Jan. 2017.

[9] Y. Shao and Y. Tang, "Fast evaluation of commutation failure risk in multi-infeed HVDC systems," *IEEE Trans. Power Syst.*, vol. 33, no.1, pp. 646-653, Jan. 2018.

[10] H. Xiao, Y. Li, J. Zhu, and X. Duan, "Efficient approach to quantify commutation failure immunity levels in multi-infeed HVDC systems," *IET Gener. Transm. Distrib.*, Mar. 2016, pp. 1032-1038.

[11] G. Li, S. Zhang, T. Jiang, H. Chen, and X. Li, "A method of detecting commutation failure in multi-infeed HVDC systems based on critical failure impedance boundary," in *Proc. IEEE PES GM*, 2017, pp. 1-5.

[12] Z. Wei, Y. Yuan, X. Lei, H. Wang, G. Sun, and Y. Sun, "Direct-current predictive control strategy for inhibiting commutation failure in HVDC converter," *IEEE Trans. Power Syst.*, vol. 29, no.5, pp. 2409-2417, Sep. 2014.

[13] S. Mirsaeidi, X. Dong, D. Tzelepis, D. Mat Said, A. Dysko, and C. Booth, "A predictive control strategy for mitigation of commutation failure in LCC-based HVDC systems," *IEEE Trans. Power Electron.*, 2018, in press.

[14] L. D. Zhang and L. Dofnas, "A novel method to mitigate commutation failures in HVDC systems," in *Proc. Int. Conf. PST*, 2002, pp. 51-56.

[15] J. Tu, Y. Pan, J. Zhang, B. Zeng, J. Jia, and J. Yi, "Transient reactive power characteristics of HVDC during commutation failure and impact of HVDC control parameters," *Journal of Engineering*, vol. 2017, no.13, pp. 1134-1139, Oct. 2017.

[16] C. H. Li, C. Liu, Z. A. Zhang, W. Yao, J. Y. Wen, and J. B. Wang, "Analysis of commutation failure in HVDC power transmission system considering prediction control of commutation failure and initial fault angle,"*Automation of Electric Power Systems*, vol. 42, no.3, pp. 56-76, Feb. 2018.

[17] C. S. Mardegan, and R. Rifaat, "Insights into applications of IEEE standards for ground-fault protection in industrial and commercial

power systems," *IEEE Trans. Industry Applications*, vol. 51, no.4, pp. 2854-2861, July-Aug. 2015.

[18] Z. Yu, J. Wen, L. Wang, W. B. Kong, and X. B. Zhao, "The study on advanced Three-pulse harmonic model of twelve-pulse converter," in *Proc. IEEE Int. Conf. PRE*, Oct. 2016, pp. 130-134.

[19] H. I. Son and H. M. Kim, "An algorithm for effective mitigation of commutation failure in high-voltage direct-current systems," *IEEE Trans. Power Delivery.*, vol. 31, no.4, pp. 1437-1446, Aug. 2016.

[20] Q. J. Chen, X. H. Wang, J. K. Liu, F. L. Song, J. S. Luo, Y. Zhang, and F. Gao, "Dynamic interaction estimation in multi-infeed system considering effects of HVDC control," in *Proc. IEEE Transportation Electrification Conf. and Expo, Asia-Pacific.*, Aug. 2017, pp. 1-5.

[21] C. Guo, Y. Liu, C. Zhao, X. Wei, and W. Xu, "Power component fault detection method and improved current order limiter control for commutation failure mitigation in HVDC," *IEEE Trans. Power Delivery*, vol. 30, no.3, pp. 1585-1593, Jun. 2015.

[22] R. Bunch and D. Kosterev, "Design and implementation of AC voltage dependent current order limiter at Pacific HVDC Intertie," *IEEE Trans. Power Delivery*, vol. 15, no.1, pp. 293-299, Jan. 2000.

[23] K. R. Padiyar, Sachchidanand, A. G. Kothari, S. Bhattacharyya, and A. Srivastava, "Study of HVDC controls through efficient dynamic digital simulation of converters," *IEEE Trans. Power Delivery*, vol. 4, no.4, pp. 2171-2178, Oct. 1989.

Wei Yao (M'13-SM'17) received the B.S. and Ph.D. degrees in electrical engineering from Huazhong University of Science and Technology (HUST), Wuhan, China, in 2004 and 2010, respectively.

He was a Post-Doctoral Researcher with the Department of Power Engineering, HUST, from 2010 to 2012 and a Postdoctoral Research Associate with the Department of Electrical Engineering and Electronics, University of Liverpool, Liverpool, U.K., from 2012 to 2014. Currently, he has been an Associate Professor with the School of Electrical and Electronics Engineering, HUST, Wuhan, China. His current research interests include power system stability analysis and control, renewable energy, HVDC and DC Grid, and application of artificial intelligence in Smart Grid.

Chang Liu received the M.S. degree in electrical engineering from Huazhong University of Science and Technology (HUST), Wuhan, China, in 2018. Since June 2018, he has been an engineer in the Electric Power Research Institute of State Grid Sichuan Electric Power Company, Chengdu, China. His current research interests include HVDC and AC\DC hybrid power systems.

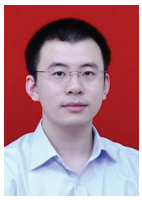

Jiakun Fang (S'10-M'13-SM'19) received the B.Sc. and Ph.D. degrees from Huazhong University of Science and Technology (HUST), China, in 2007 and 2012, respectively.

He was with the Department of Energy Technology, Aalborg University, Aalborg, Denmark from 2012 to 2019. Currently, he is a Professor in Huazhong University of Science and Technology (HUST), Wuhan, China His research interests include power system dynamic stability control, power grid complexity analysis, and integrated energy system.

Xiaomeng Ai (S'11-M'17) received the B.Eng degree in mathematics and applied mathematics and Ph.D. in electrical engineering in 2008 and 2014, respectively, both from Huazhong University of Science and Technology (HUST), Wuhan, China.

Currently he is a lecturer at HUST. His research interests include robust optimization theory in power system, renewable energy integration, and integrated energy market.

Jinyu Wen (M'10) received the B.S. and Ph.D. degrees in electrical engineering from Huazhong University of Science and Technology (HUST), Wuhan, China, in 1992 and 1998, respectively.

He was a Visiting Student from 1996 to 1997 and Research Fellow from 2002 to 2003 all at the University of Liverpool, Liverpool, UK, and a Senior Visiting Researcher at the University of Texas at Arlington, Arlington, USA, in 2010. From 1998 to 2002 he was a Director Engineer with XJ Electric Co. Ltd. in China. In 2003, he joined the HUST and now is a Professor with the School of Electrical and Electronics Engineering, HUST. His current research interests include renewable energy integration, energy storage, multi-terminal HVDC, and power system operation and control.

Shijie Cheng (M'86-SM'87-F'11-LF'18) received the B.S. degree from Xi'an Jiaotong University, Xi'an, China, in 1967, the M.Sc. degree from Huazhong University of Science and Technology (HUST), Wuhan, China, in 1981, and the Ph.D. degree from the University of Calgary, Calgary, AB, Canada, in 1986, all in the electrical engineering.

He has been a Professor with the School of Electrical and Electronics Engineering, HUST, Wuhan, China, since 1991. His research interests are power system control, stability analysis, application of Artificial Intelligence, and energy storage.

Prof. Cheng is a Fellow of the Chinese Academy of Sciences.